J Therm Anal Calorim (2012) 108:1235–1242
DOI 10.1007/s10973-011-1799-8

Preparation of $LiZnPO_4 \cdot H_2O$ via a novel modified method and its non-isothermal kinetics and thermodynamics of thermal decomposition

Zhipeng Chen · Qian Chai · Sen Liao · Yu He · Wenwei Wu · Bin Li

Received: 14 April 2011 / Accepted: 8 July 2011 / Published online: 26 July 2011
© Akadémiai Kiadó, Budapest, Hungary 2011

Abstract The single phase α-$LiZnPO_4 \cdot H_2O$ was directly synthesized via solid-state reaction at room temperature using $LiH_2PO_4 \cdot H_2O$, $ZnSO_4 \cdot 7H_2O$, and Na_2CO_3 as raw materials. XRD analysis showed that α-$LiZnPO_4 \cdot H_2O$ was a compound with orthorhombic structure. The thermal process of α-$LiZnPO_4 \cdot H_2O$ experienced two steps, which involved the dehydration of one crystal water molecule at first, and then the crystallization of $LiZnPO_4$. The DTA curve had the one endothermic peak and one exothermic peak, respectively, corresponding to dehydration of α-$LiZnPO_4 \cdot H_2O$ and crystallization of $LiZnPO_4$. Based on the iterative iso-conversional procedure, the average values of the activation energies associated with the thermal dehydration of α-$LiZnPO_4 \cdot H_2O$, was determined to be 86.59 kJ mol^{-1}. Dehydration of the crystal water molecule of α-$LiZnPO_4 \cdot H_2O$ is single-step reaction mechanism. A method of multiple rate iso-temperature was used to define the most probable mechanism $g(\alpha)$ of the dehydration step. The dehydration step is contracting cylinder model ($g(\alpha) = 1-(1-\alpha)^{1/2}$) and is controlled by phase boundary reaction mechanism. The pre-exponential factor A was obtained on the basis of E_a and $g(\alpha)$. Besides, the thermodynamic parameters ($\Delta S^{\neq}$, $\Delta H^{\neq}$, and $\Delta G^{\neq}$) of the dehydration reaction of α-$LiZnPO_4 \cdot H_2O$ were determined.

Keywords α-$LiZnPO_4 \cdot H_2O$ · Non-isothermal kinetics · Thermodynamics · Thermal decomposition · Solid-state reaction at room temperature

Z. Chen · Q. Chai · S. Liao (✉) · Y. He · W. Wu · B. Li
School of Chemistry and Chemical Engineering, Guangxi University, Nanning 530004, Guangxi, People's Republic of China
e-mail: liaosen@gxu.edu.cn

Introduction

The synthesis and structural characterization of zinc phosphates have received considerable amount of attention because of their potential applications as new materials that may have ion exchange, absorption, separation, ionic conductivity, and heterogeneous catalytic properties [1–9].

A water-containing lithium zinc phosphate, $LiZnPO_4 \cdot H_2O$ [5, 6], was described having a zeolite type ABW structure, i.e., isomorphous with zeolite Li-A(BW), $LiAlSiO_4 \cdot H_2O$. Hydrothermal techniques have been used for the preparation of the $LiZnPO_4 \cdot H_2O$ [5, 6].

Solid-state reaction at room temperature or near room temperature was a novel synthetic technique which has been developed in recent decade [10–23]. Recently, we successfully used this novel technique to synthesize α-$LiZnPO_4 \cdot H_2O$ with $LiH_2PO_4 \cdot H_2O$, and $ZnCO_3$ as raw materials [22].

Wu and Jiang [23] prepared $ZnCO_3$ via solid-state reaction at room temperature with $ZnSO_4 \cdot 7H_2O$ and NH_4HCO_3 as raw materials. Therefore, it suggested that the α-$LiZnPO_4 \cdot H_2O$ can be directly synthesized via the modified method using $LiH_2PO_4 \cdot H_2O$, $ZnSO_4 \cdot 7H_2O$, and Na_2CO_3 as raw materials.

So, as a part of the system research, the aim of this study was to prepare single phase α-$LiZnPO_4 \cdot H_2O$ via the above method with $LiH_2PO_4 \cdot H_2O$, $ZnSO_4 \cdot 7H_2O$, and Na_2CO_3 and to study the kinetics and thermodynamics of the decomposition of α-$LiZnPO_4 \cdot H_2O$ using TG–DTA technique. Non-isothermal kinetics of the decomposition process of α-$LiZnPO_4 \cdot H_2O$ was interpreted by a modified method [24–29], the apparent activation energy E_a was obtained from iterative procedure [29], the most probable mechanism function $g(\alpha)$ of the thermal decomposition reaction was deduced from multiple rate iso-temperature

method, pre-exponential factor A was calculated on the basis of E_a and $g(\alpha)$ subsequently. The kinetic (E_a, A, mechanism) and thermodynamic parameters ($\Delta H^{\neq}$, $\Delta S^{\neq}$, $\Delta G^{\neq}$) of the dehydration reaction of α-$LiZnPO_4{\cdot}H_2O$ were discussed for the first time.

Experiment

Reagent and apparatus

All chemicals were of reagent grade purity. TG/DTA measurements were made using a Netsch 40PC thermogravimetric analyzer. Samples of 50 mg mass were used for the experiments varied out at heating rates of 5, 10, 15, 20 °C min^{-1} up to 800 °C. Pure gas was argon gas of high purity, flowing at 20 mL min^{-1}. The samples were loaded without pressing into an alumina crucible, α-alumina calcined up to 1373 K was used as a standard reference material. (The results presented in the article were calculated by the programs compiled by ourselves).

X-ray powder diffraction (XRD) was performed at a scanning rate of 5° min^{-1} from 5° to 65° for 2θ at room temperature using a Rigaku D/max 2500 V diffractometer equipped with a graphite monochromator and a Cu target. Fourier transform infrared (FTIR) spectroscopy using a Nicolet NEXUS-470 spectrometer in the wavenumbers range of 400–4000 cm^{-1}. The FTIR spectra were taken on KBr pellets. The morphology of the product and its calcined samples were examined by S-3400 scanning electron microscopy (SEM). The samples were mounted on an aluminum slice then coated with Au.

Preparation of α-$LiZnPO_4{\cdot}H_2O$

The lithium zinc phosphate hydrate α-$LiZnPO_4{\cdot}H_2O$ was prepared by solid-state reaction at room temperature using $LiH_2PO_4{\cdot}H_2O$, $ZnSO_4{\cdot}7H_2O$, and Na_2CO_3 as starting materials. In a typical synthesis: first, $LiH_2PO_4{\cdot}H_2O$ (31.5 mmol, 3.84 g), $ZnSO_4{\cdot}7H_2O$ (30.0 mmol, 8.64 g), and surfactant polyethylene glycol-400 (PEG-400) (1.5 mL) were put in a mortar, and ground to form uniform mixture. Then after powder of Na_2CO_3 (30.0 mmol, 3.18 g) was added into the mixture, and the mixture was fully ground for 30 min. The reactant mixture gradually became damp, and then a paste formed quickly. The reaction mixture was kept at room temperature for 4 h. The mixture was washed with deionized water to remove soluble inorganic salts until SO_4^{2-} ion could not be visually detected with a 0.5 mol L^{-1} $BaCl_2$ solution. The solid was then washed with a small amount of anhydrous ethanol and dried at 80 °C for 3 h to give the single phase α-$LiZnPO_4{\cdot}H_2O$.

Method of determining kinetic parameters, model function, and thermodynamic parameters

Theoretical

Kinetic equation of solid-state reaction can be expressed as Eq. 1:

$$\frac{d\alpha}{dt} = A\exp\left(-\frac{E_a}{RT}\right)f(\alpha) \tag{1}$$

When heating rate is kept constant, that is: $q = dT/dt$. Equation 1 can be rewritten into the Eq. 2:

$$\frac{d\alpha}{dT} = \frac{A}{q}\exp\left(-\frac{E_a}{RT}\right)f(\alpha) \tag{2}$$

Rearranging Eq. 2, one obtains:

$$\frac{d\alpha}{f(\alpha)} = \frac{A}{q}\exp\left(-\frac{E_a}{RT}\right)dT \tag{3}$$

where E_a is apparent activation energy, q is the heating rate (5, 10, 15, 20 °C min^{-1}), A is pre-exponential factor, R is the gas constant, α is called conversion degree.

Calculation of activation energy by iterative procedure

From Eq. 3, OFW equation [30–32] and KAS [33, 34] equation are deduced.

OFW equation:

$$\ln q = \ln\frac{0.0048AE_a}{g(\alpha)R} - 1.0516\frac{E_a}{RT} \tag{4}$$

KAS equation:

$$\ln\frac{q}{T^2} = \ln\frac{AR}{g(\alpha)E_a} - \frac{E_a}{RT} \tag{5}$$

The iterative procedure [26–28, 35] is used to calculate the approximate value of E_a approach to the exact value, the Equations are expressed:

$$\ln\frac{q}{H(x)} = \ln\frac{0.0048AE_a}{g(\alpha)R} - 1.0516\frac{E_a}{RT} \tag{6}$$

and

$$\ln\frac{q}{h(x)T^2} = \ln\frac{AR}{g(\alpha)E_a} - \frac{E_a}{RT} \tag{7}$$

Because

$$g(\alpha) = \int_0^{\alpha}\frac{d\alpha}{f(\alpha)} \approx \frac{A}{q}\int_0^{T} e^{-E_a/RT}dT = \frac{AE_a e^{-x}}{qRx^2}h(x) \tag{8}$$

and where $h(x)$ is expressed by the fourth Senum and Yang approximation formulae [28, 36]:

$$h(x) = \frac{x^4 + 18x^3 + 86x^2 + 96x}{x^4 + 20x^3 + 120x^2 + 240x + 120} \quad (9)$$

where $x = E_a/RT$ and $H(x)$ is equal to:

$$H(x) = \frac{\exp(-x)h(x)/x^2}{0.0048\ \exp(-1.0516x)} \quad (10)$$

The iterative procedure performed involved the following steps [25, 26]: (i) Assume $h(x) = 1$ or $H(x) = 1$ to estimate the initial value of the activation energy E_{a1}. The conventional iso-conversional methods stop the calculation at this step; (ii) using E_{a1}, calculate a new value of E_{a2} for the activation energy from the plot of $\ln[q/H(x)]$ versus $1/T$ or $\ln[q/h(x)T^2]$ versus $1/T$; (iii) repeat step (ii), replacing E_{a1} with E_{a2}. When $E_{ai} - E_{a(i-1)} < 0.01$ kJ mol^{-1}, the last value of E_{ai} was considered to be the exact value of the activation energy of the reaction. These plots are model independent since the estimation of the apparent activation energy does not require selection of particular kinetic model (type of $g(\alpha)$ function). Therefore, the activation energy values obtained by this method are usually regarded as more reliable than these obtained by a single TG curve.

Determination of the most probably mechanism function

The following equation is used to estimate the most correct reaction mechanism, i.e., $g(\alpha)$ function [26]:

$$\ln g(\alpha) = \left[\ln\frac{AE_a}{R} + \ln\frac{e^{-x}}{x^2} + \ln h(x)\right] - \ln q \quad (11)$$

The conversions α corresponding multiple rates at the same temperature are put into the left of Eq. 11, combined with thirty-one types of mechanism functions [26], the slope k and correlation coefficient r are obtained from the plot of $\ln[g(\alpha)]$ versus $\ln q$. The probable mechanism function is that for which the value of the slope k is near to -1.00000 and correlation coefficient r is better. If several $g(\alpha)$ answer for this requirement, the conversions α corresponding to multiple rates at several the same temperatures are applied to calculate the probable mechanism by the same method, the most probable mechanism function is that for which among the results of k and r, the value of k is closest to -1.00000 and the correlation coefficient is higher.

Calculation of pre-exponential factor A

The pre-exponential factor A can be estimated from the intercept of the plots of Eqs. 6 and 7, inserting the most probable $g(\alpha)$ function determined [25].

Calculation of thermodynamic parameters of thermal decomposition reaction [37, 38]

The change of the entropy ($\Delta S^{\neq}$) may be calculated according to the Eq. 12:

$$\Delta S^{\neq} = R\ln\left(\frac{Ah}{e\chi k_B T_P}\right) \quad (12)$$

where A is the pre-exponential factor, $e = 2.7183$ is the Neper number, χ is the transition factor, which is unity for monomolecular reactions, k_B is the Boltzmann constant (1.381×10^{-23} J K^{-1}), h is the Plank constant (6.626×10^{-34} J s); T_P is the peak temperature in DTG curve, R is the gas constant (8.314 J mol^{-1} K^{-1}).

The change of the enthalpy ($\Delta H^{\neq}$) may be obtained according to the Eq. 13:

$$\Delta H^{\neq} = E^{\neq} - RT_P \quad (13)$$

where $E^{\neq}$ is the activation energy, E_a, obtained from the iterative procedure of KAS method.

The change of Gibbs free energy $\Delta G^{\neq}$ for the decomposition reaction can be calculated using the well-known thermodynamic Eq. 14:

$$\Delta G^{\neq} = \Delta H^{\neq} - T_p\Delta S^{\neq} \quad (14)$$

Results and discussion

XRD analysis of the product and its calcined samples

Figure 1 shows the XRD patterns of the product dried at 80 °C and the product resulting from calcination at 650 °C for 2 h.

From Fig. 1a, the results show that all diffraction peaks in the pattern could be indexed to obtain lattice parameters: $a = 10.52716(7)$ Å, $b = 8.11728(6)$ Å, and $c = 5.02327(5)$ Å; $\alpha = \beta = \gamma = 90^o$ that are in agreement with that of orthorhombic $LiZnPO_4 \cdot H_2O$, with space group Pna21(33) and cell parameters: $a = 10.575$ Å, $b = 8.076$ Å, and $c = 4.994$ Å, and $\alpha = \beta = \gamma = 90^o$, from PDF card 83-0263. No diffraction peaks of other impurities, such as $Zn_3(PO_4)_2 \cdot 4H_2O$ and $NaZnPO_4 \cdot H_2O$, are observed, which indicates that the single phase α-$LiZnPO_4 \cdot H_2O$ [5] is synthesized by solid-state reaction at room temperature. It is obvious that the synthesis described here is a modified one and also more convenient one when compared with that reported by us [22]. From Fig. 1b, all the diffraction peaks in the XRD pattern are found to be in agreement with that of monoclinic $LiZnPO_4$, space group Cc (9), from PDF card 79-0804.

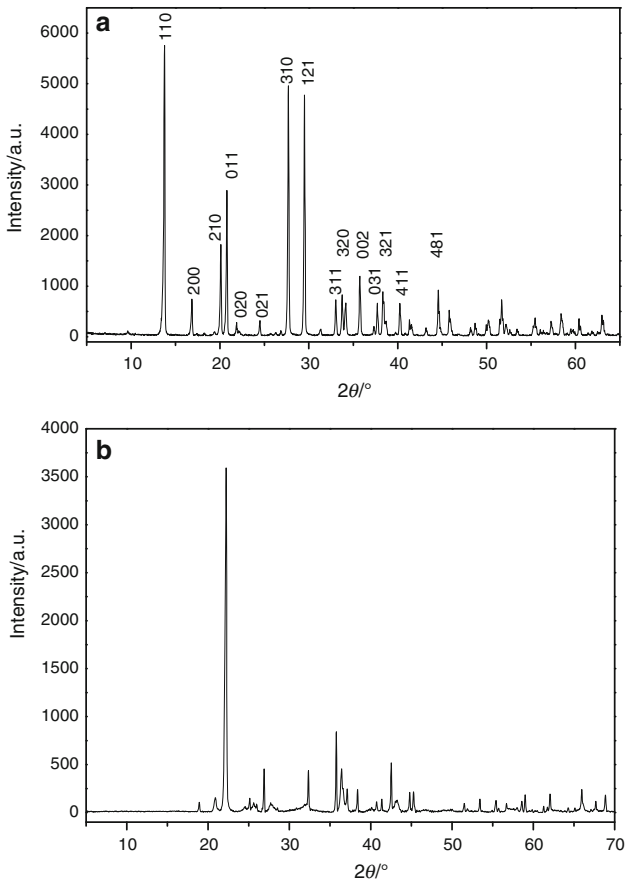

Fig. 1 XRD patterns of the product (**a**) and its calcined product (**b**) at 650 °C for 2 h

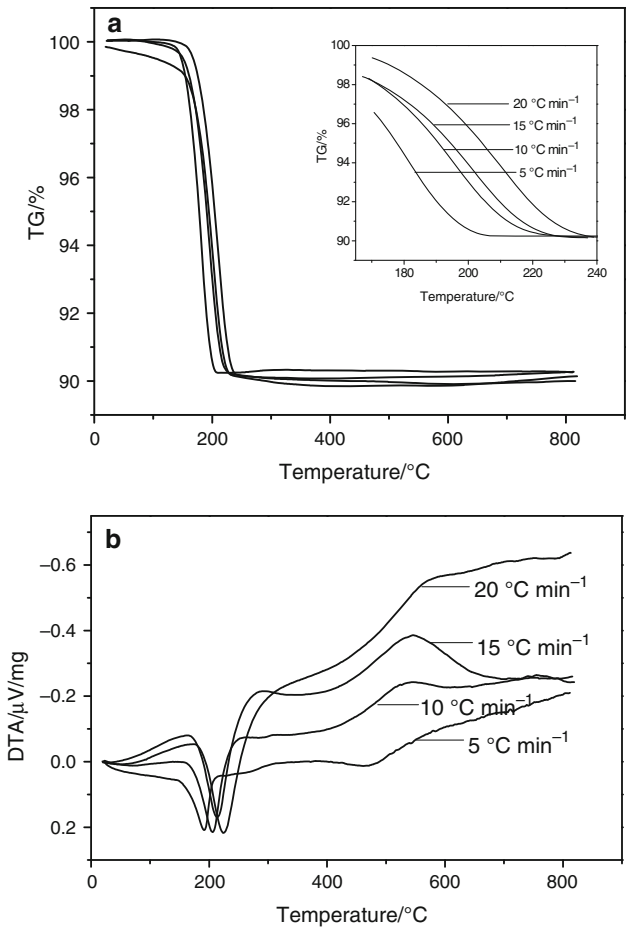

Fig. 2 TG/DTA curves of the $LiZnPO_4{\cdot}H_2O$ at different heating rates

TG/DTA analysis of the synthetic product

Figure 2 shows the TG/DTA curves of the synthetic product at four different heating rates from ambient temperature to 800 °C, respectively.

The TG curves show that thermal decomposition of the α-$LiZnPO_4{\cdot}H_2O$ below 800 °C occurs in one well-defined step. The mass loss starts at about 120 °C, ends at about 270 °C, and characterized by a strong endothermic DTA peak at about 200 °C that can be attributed to dehydration from α-$LiZnPO_4{\cdot}H_2O$ and the formation of $LiZnPO_4$. The observed mass loss in the TG curve is 9.71%, which is in good agreement with 9.72% theoretic mass loss of one water molecule eliminated from α-$LiZnPO_4{\cdot}H_2O$. The exothermic DTA peak at about 545 °C can be attributed to the phase change from amorphous $LiZnPO_4$ to monoclinic $LiZnPO_4$.

IR spectroscopic analysis of the product and its calcined samples

FT–IR spectra of the prepared and its calcined samples are shown in Fig. 3. From Fig. 3a, the strong band of the prepared sample at 1064 cm^{-1} is attributed to the O–P tetrahedron vibration. The bending OPO vibrations appear in the region of 500–627 cm^{-1}. The strong and broad band around 3000–3600 cm^{-1} is assigned to the stretching OH vibration of the water molecule, while the band observed at 1607 cm^{-1} is assigned to the bending mode of the HOH. It can be seen from Fig. 3b that the intensity of bands at 2300–3600 and 1607 cm^{-1} disappear after calcination. It is explained by the fact that α-$LiZnPO_4{\cdot}H_2O$ finish elimination of its crystal water after calcination.

SEM analysis of the synthetic product and its calcined samples

The morphology of α-$LiZnPO_4{\cdot}H_2O$ and its calcined sample are shown in Fig. 4. From Fig. 4a, it can be seen that the α-$LiZnPO_4{\cdot}H_2O$ sample is composed of prisms. Figure 4b shows the SEM micrographs of samples obtained at 650 °C. It can be seen that the morphology of the sample has been became block-like shapes, and there is soft agglomeration phenomenon among one particle of sample.

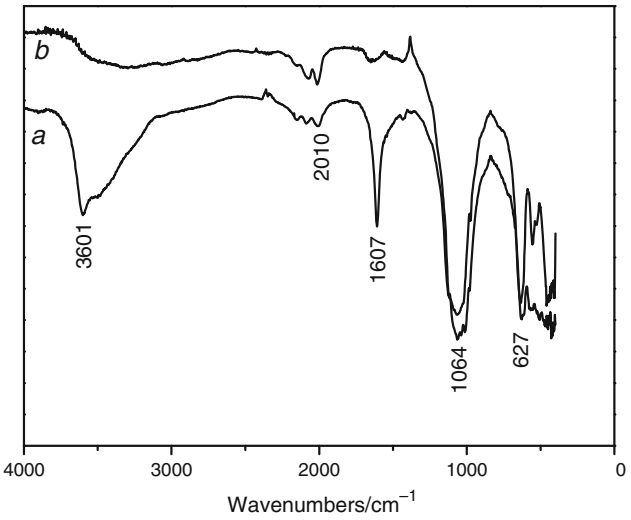

Fig. 3 The infrared spectroscopy of the product (**a**) and its calcined product (**b**) at 650 °C for 2 h

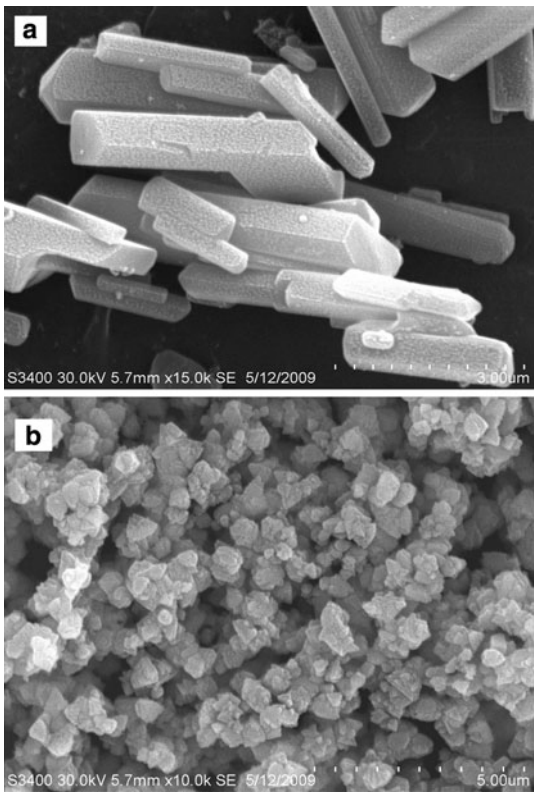

Fig. 4 SEM image of the product (**a**) and its calcined product (**b**) at 650 °C for 2 h

Thermal decomposition kinetics

In accordance with TG/DTA analysis and XRD analysis of the synthetic product, and its calcined product mentioned above, thermal process of α-$LiZnPO_4 \cdot H_2O$ below 800 °C consists of two steps, which can be expressed as follows:

$$\alpha - LiZnPO_4 \cdot H_2O\ (cr) \rightarrow LiZnPO_4\ (am) + H_2O\ (g)$$

$$LiZnPO_4\ (am) \rightarrow LiZnPO_4\ (cr)$$

Above two steps involve the dehydration of one crystal water molecule at first, and then the crystallization of $LiZnPO_4$. The dehydration step will be studied using non-isothermal method in this article.

According to the non-isothermal method, the basic data of α and T collected from the TG curves of the thermal decomposition of α-$LiZnPO_4 \cdot H_2O$ at various heating rates (5, 10, 15, and 20 °C min^{-1}) are illustrated in Table 1.

Table 1 Temperatures corresponding to conversion degrees at various heating rates

Conversion degree/a	Heating rate/°C min^{-1}			
	T/K			
	5	10	15	20
0.2	434.78	445.11	444.10	458.40
0.3	440.79	452.39	453.70	465.84
0.4	445.62	458.15	460.76	471.91
0.5	449.97	463.23	467.66	476.55
0.6	453.87	468.03	472.66	481.36
0.7	457.81	472.67	477.54	486.12
0.8	462.06	477.31	482.76	491.13

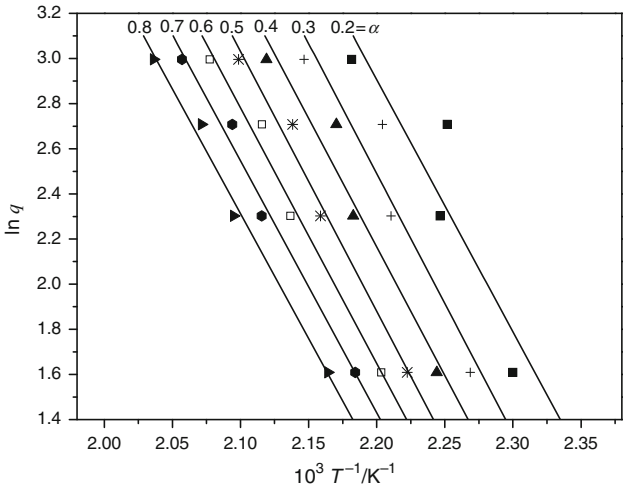

Fig. 5 Isoconversional plots at various conversion degrees for $LiZnPO_4 \cdot H_2O$ draw according OFW calculation procedure

Calculation of activation energy E_a by iterative procedure

According to Eqs. 4 and 5, the iso-conversional calculation procedures of OFW and KAS were used. The corresponding

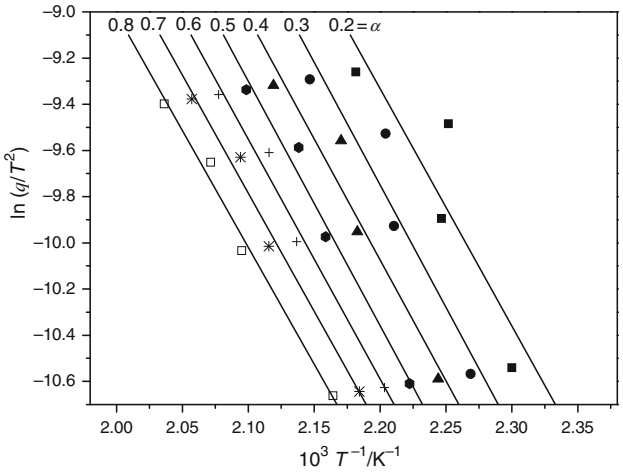

Fig. 6 Isoconversional plots at various conversion degrees for $LiZnPO_4{\cdot}H_2O$ draw according KAS calculation procedure

OFW lines and KAS lines obtained at different conversion degrees α and different heating rates q are shown in Figs. 5 and 6, respectively.

The values of E_a of the dehydration of α-$LiZnPO_4{\cdot}H_2O$ corresponding to different conversions α are obtained by the OFW and KAS calculation procedure and the above iterative method, and shown in Table 2.

As shown in Table 2, compared with the values of E_a obtained by interative method and OFW or KAS method, that obtained by OFW method is general higher (excessing about 2.57–3.09 kJ mol^{-1}), however, the results obtained by iterative method and KAS method are very close to each other (differing about 0.28 kJ mol^{-1}). Meanwhile, it can be discovered that the values obtained from the plot of $\ln[q/H(x)]$ versus $1/T$ or $\ln[q/(h(x)T^2)]$ versus $1/T$ by interative procedure are very close to each other. It is obvious that the values of E_a obtained from iterative method or KAS method are more reliable, so the suggestion that the values obtained from the two methods determined the range of E_a is reasonable, while the heating rates are 5, 10, 15, 20 °C min^{-1}, the value of E_a is equal to 86.59 kJ mol^{-1} at $0.20 < \alpha < 0.80$. From Table 2, it is seen activation energies at different conversion degree, varies here by only about 2.1%, indicating that a single-step kinetic process takes place in thermal dehydration reaction.

Determination of the most probably mechanism function

Determination of the most probably mechanism function by multiple rate iso-temperature method roughly

The conversions for $q = 5$, 10, 15, 20 °C min^{-1} at the same temperature are illustrated in Table 3. An appropriate temperature is randomly selected; the range of the conversions of this temperature should be within 0.10–0.90. We choose the corresponding conversions of $T = 454$ K for example to put into thirty-one types of mechanism functions [26]. The slope k, correlation coefficient r, and intercept B of linear regression of $\ln[g(\alpha)]$ versus $\ln q$ are obtained. The results of the linear regression show that the slopes of No. 13 and 14 mechanism function are closer to -1.00000 than others and with better correlation coefficient r, but which type of mechanism is the most probable one, it needs further research.

Determination of the most probably mechanism function by multiple rate iso-temperature method precisely

We randomly choose several temperatures (Table 3) which corresponding conversions $0.1 < \alpha < 0.9$ to calculate the slope k, correlation coefficient r, and intercept B of No. 13 and 14 mechanism function by the same method. The

Table 2 The activation energies for thermal decomposition of α-$LiZnPO_4{\cdot}H_2O$, E_a (kJ mol^{-1}), and the intercept, B, at different conversion degree and calculating procedure

Conversion degree/α	E_a/kJ mol^{-1}				B	
	OFW method	KAS method	$\ln[q/H(x)] \sim 1/T$	$\ln[q/(h(x)T^2)] \sim 1/T$	Eq. 6	Eq. 7
0.2	88.33	85.46	85.73	85.73	26.57440	13.43152
0.3	91.04	88.21	88.47	88.47	26.94590	13.73985
0.4	90.07	87.09	87.37	87.37	26.30391	13.12306
0.5	91.02	88.02	88.30	88.30	26.28595	13.08382
0.6	89.46	86.32	86.60	86.60	25.56902	12.40566
0.7	88.29	85.02	85.31	85.31	24.97933	11.84614
0.8	87.45	84.06	84.36	84.36	24.48286	11.37209
Average	89.38	86.31	86.59	86.59		

$\ln[q/H(x)] \sim 1/T$ is the iterative results of OFW method and $\ln[q/(h(x)T^2)] \sim 1/T$ is the iterative results of KAS method, respectively

B is the intercept of the plots of Eqs. 6 and 7

Table 3 The relation of temperature and conversion α at different heating rates q (°C min^{-1})

T/K	α			
	$q = 5$	$q = 10$	$q = 15$	$q = 20$
451	0.52616	0.27798	0.26789	0.12126
452	0.55259	0.29344	0.27914	0.13067
453	0.57822	0.30946	0.29128	0.14062
454	0.60379	0.32602	0.30388	0.15091
455	0.62924	0.34309	0.31644	0.16129
456	0.65529	0.36065	0.32996	0.17226
457	0.68023	0.37866	0.34396	0.18361
459	0.72896	0.41594	0.37284	0.20712
461	0.77637	0.45473	0.40363	0.23217
463	0.82033	0.49481	0.43703	0.25915
465	0.86162	0.53597	0.44976	0.28750

Table 4 lng(α) versus ln$q$ curves of two types of probable mechanism functions when $0.1 < \alpha < 0.9$

T/K	Function No.	B	$-k$	$-r$
451	13	0.22302	1.05660	0.93994
	14	0.51929	1.02382	0.93786
452	13	0.27984	1.05425	0.94566
	14	0.56816	1.01901	0.94357
453	13	0.32976	1.04938	0.95030
	14	0.61005	1.01168	0.94820
454	13	0.37938	1.04486	0.95440
	14	0.65121	1.00457	0.95229
455	13	0.43114	1.04204	0.95829
	14	0.69403	0.99900	0.95616
456	13	0.48352	1.03935	0.96161
	14	0.73673	0.99331	0.95947
457	13	0.53135	1.03535	0.96443
	14	0.77472	0.98629	0.96228

results are listed in Table 4, they illustrate that the slope of No. 14 is the most adjacent to −1.00000 and correlation coefficient r is better. So we can determine that No. 14 mechanism function is the most probable one of the dehydration of α-$LiZnPO_4 \cdot H_2O$, with integral form $g(\alpha) = 1-(1-\alpha)^{1/2}$, belongs to the mechanism of phase boundary reaction, R_2.

Calculation of pre-exponential factor A

The pre-exponential factor A were estimated from the intercept of the plots of Eq. 7 (the intercept, B, was shown in Table 2), inserting the most probable $g(\alpha)$ function determined (No. 14). The results showed that the range of pre-exponential factor A was $0.8120 \times 10^7 - 2.6859 \times 10^7$ s^{-1}, and average $A = 1.6915 \times 10^7$ s^{-1}.

Determination of thermodynamic parameters of thermal decomposition reaction

Thermodynamic parameters ($\Delta S^{\neq}$, $\Delta H^{\neq}$, and $\Delta G^{\neq}$) were calculated from Eqs. 12–14. The average values of the parameters were $\Delta S^{\neq} = -119.33$ J mol^{-1} K^{-1}, $\Delta H^{\neq} = 82.677$ kJ mol^{-1}, and $\Delta G^{\neq} = 138.869$ kJ mol^{-1}. As can be seen from the results, the values of $\Delta S^{\neq}$ for the dehydration step are negative. The positive values of $\Delta G^{\neq}$ at this step are due to the fact that dehydration of the crystal waters of α-$LiZnPO_4 \cdot H_2O$ is not spontaneous at room temperature.

Conclusions

This study has successfully achieved a directly synthesis of single phase α-$LiZnPO_4 \cdot H_2O$ via solid-state reaction at room temperature using $LiH_2PO_4 \cdot H_2O$, $ZnSO_4 \cdot 7H_2O$, and Na_2CO_3 as raw materials. The thermal process of α-$LiZnPO_4 \cdot H_2O$ in the range of ambient temperature to 800 °C is a two step process, which involves the dehydration of the one crystal water molecule at first, and then crystallization of $LiZnPO_4$. The kinetics of the dehydration step of α-$LiZnPO_4 \cdot H_2O$ was studied using iterative procedure, Ozawa–Flynn–Wall (OFW) method, and the Kissinger–Akahira–Sunose (KAS) method. Based on the iterative iso-conversional procedure, the average values of the activation energies associated with the thermal dehydration of α-$LiZnPO_4 \cdot H_2O$, was determined to be 86.59 kJ mol^{-1}. Dehydration of the crystal water molecule of α-$LiZnPO_4 \cdot H_2O$ is single-step reaction mechanism. A method of multiple rate iso-temperature was used to define the most probable mechanism $g(\alpha)$ of the dehydration step. The dehydration step is contracting cylinder model ($g(\alpha) = 1-(1-\alpha)^{1/2}$) and is controlled by phase boundary reaction mechanism. The pre-exponential factor A is obtained on the basis of E_a and $g(\alpha)$. The thermodynamic parameters ($\Delta S^{\neq}$, $\Delta H^{\neq}$, and $\Delta G^{\neq}$) of the dehydration reaction of α-$LiZnPO_4 \cdot H_2O$ are obtained. These data will be important for further studies of the studied compound, and to solve various scientific and practical problems involving the participation of solid phases.

Acknowledgements This study was financially supported by the Key laboratory of new processing technology for nonferrous metals and materials, Ministry of Education, Guangxi University (No. GXKFZ-02), the Guangxi Natural Scientific Foundation of China (Grant No. 0991108 and. 0832111), and the Guangxi Science and Technology Agency Research Item of China (Grant No. 0895002–9).

References

1. Vasovic DD, Stojakovic DR. Metal phosphate preparation using boron phosphate. Mater Res Bull. 1997;32:779–84.
2. Chen J, Natarajan S, Thomas JM, Jones RH, Hursthouse MB. A novel open-framework cobalt phosphate containing a tetrahedrally coordinated cobalt(II) center: $CoPO_4{\cdot}0.5C_2H_{10}N_2$. Angew Chem Int Ed. 1994;33:639–40.
3. Gier TE, Stucky GD. Low-temperature synthesis of hydrated zinco(beryllo)-phosphate and arsenate molecular sieves. Nature. 1991;349:508–10.
4. Ng HY, Harrison WTA. Monoclinic $NaZnPO_4$-ABW, a new modification of the zeolite ABW structure type containing elliptical eight-ring channels. Micropor Mesopor Mater. 1998;23:197–202.
5. Harrison WTA, Gier TE, Nicol JM, Stucky GD. Tetrahedral-framework lithium zinc phosphate phases: location of light-atom positions in $LiZnPO_4{\cdot}H_2O$ by powder neutron diffraction and structure determination of $LiZnPO_4$ by ab initio methods. J Solid State Chem. 1995;114:249–57.
6. Jensen TR. A new polymorph of $LiZnPO_4{\cdot}H_2O$: synthesis, crystal structure and thermal transformation. J Chem Soc Dalton Trans. 1998;18:2261–6.
7. Bu XH, Gier TE, Stucky GD. A new polymorph of lithium zinc phosphate with the cristobalite-type framework topology. J Solid State Chem. 1998;138:126–30.
8. Bensalem A. Synthesis and characterization of a new layered lithium zinc phosphate hydrate. J Solid State Chem. 2001;162:29–33.
9. Jensen TR, Hazell RG, NØrlund Christensen A, Hanson JC. Hydrothermal synthesis of lithium zinc phosphates: Structural investigation of twinned α-$Li_4Zn(PO_4)_2$ and a high temperature polymorph β-$Li_4Zn(PO_4)_2$. J Solid State Chem. 2002;166:341–51.
10. Xin XQ, Zheng LM. Solid state reactions of coordination compounds at low heating temperatures. J Solid State Chem. 1993;106:451–60.
11. Lang JP, Xin XQ. Solid state synthesis of Mo(W)-S cluster compounds at low heating temperatures. J Solid State Chem. 1994;108:118–27.
12. Yao XB, Zheng LM, Xin XQ. Synthesis and characterization of solid-coordination compounds $Cu(AP)_2Cl_2$. J Solid State Chem. 1995;117:333–6.
13. Li QW, Luo GA, Shu YQ. Response of nanosized cobalt oxide electrodes as pH sensors. Anal Chim Acta. 2000;409:137–42.
14. Cao YL, Liu L, Jia DZ, Xin XQ. One-step solid-state synthesis and characterization of two kinds of $ZnC_2O_4{\cdot}2H_2O$ hollow nanostructures. Chin J Chem. 2005;23:539–42.
15. Cao YL, Jia DZ, Liu L, Luo JM. Rapid synthesis of lead oxide nanorods by one-step solid-state chemical reaction at room temperature. Chin J Chem. 2004;22:1288–90.
16. Pawlig O, Trettin R. Synthesis and characterization of α-hopeite, $Zn_3(PO_4)_2{\cdot}4H_2O$. Mater Res Bull. 1999;34:1959–66.
17. Kowalak S, Jankowska A, Baran E. Spontaneous crystallization of zincophosphate sodalite by means of dry substrate grinding. Chem Commun. 2001;6:575–6.
18. Liao S, Wu WW, Sun YB, Song BL. A simple and novel route for the preparation of chiral sodium zincophosphate. Chin J Chem. 2008;26:281–5.
19. Yu H, Xu QF, Sun ZR, Ji SJ, Chen JX, Liu Q, Lang JP, Tatsumi K. Unique formation of two different W/Ag/S clusters from the same components via a low heating temperature solid state reaction and a solution reaction and their third-order NLO properties in solution. Chem Commun. 2001;1:2614–5.
20. Chen JX, Xu QF, Xu Y, Zhang Y, Chen ZN, Lang JP. Solid-state reactions of AgAc with $TabHPF_6$ at room temperature-isolation and structural characterisation of an unusual octadecanuclear silver thiolate cluster $[Ag_9(Tab)_8(MeCN)_8]_2$ $(PF_6)_{18}{\cdot}4MeCN$ [Tab = 4-(trimethylammonio)benzenethiolate]. Eur J Inorg Chem. 2004;2004:4247–52.
21. Chen JX, Tang XY, Chen Y, Zhang WH, Li LL, Yuan RX, Zhang Y, Lang JP. Formation of four different $[MoOS_3Cu_3]$-based coordination polymers from the same components via four synthetic routes. Cryst Growth Des. 2009;9:1461–9.
22. Liao S, Chen ZP, Tian XZ, Wu WW. Synthesis and regulation of α-$LiZnPO_4{\cdot}H_2O$ via a solid state reaction at low-heating temperatures. Mater Res Bull. 2009;44:1428–31.
23. Wu WW, Jiang QY. Preparation of nanocrystalline zinc carbonate and zinc oxide via solid state reaction at room temperature. Mater Lett. 2006;60:2791–4.
24. Vyazovkin S, Burnham AK, Criado JM, Pérez-Maqueda LA, Popescu C, Sbirrazzuoli N. ICTAC kinetics committee recommendations for performing kinetic computations on thermal analysis data. Thermochim Acta. 2011;520:1–19.
25. Genieva SD, Vlaev LT, Atanassov AN. Study of the thermo-oxidative degradation kinetics of poly(tetrafluoroethene) using iso-conversional calculation procedure. J Therm Anal Calorim. 2010;99:551–61.
26. Liqing L, Donghua C. Application of iso-temperature method of multiple rate to kinetic analysis. Dehydration for calcium oxalate monohydrate. J Therm Anal Calorim. 2004;78:283–93.
27. Chunxiu G, Yufang S, Donghua C. Comparative method to evaluate reliable kinetic triplets of thermal decomposition reactions. J Therm Anal Calorim. 2004;76:203–16.
28. Gao Z, Amasaki I, Nakada M. A description of kinetics of thermal decomposition of calcium oxalate monochydrate by means of the accommodated Rn model. Thermochim Acta. 2002;385:95–103.
29. Gao X, Dollimore D. The thermal decomposition of oxalates: part 26. A kinetic study of the thermal decomposition of manganese(II) oxalate dehydrate. Thermochim Acta. 1993;215:47–63.
30. Ozawa T. A new method of analyzing thermogravimetric data. Bull Chem Soc Jpn. 1965;38:1881–6.
31. Paik P, Kar KK. Kinetics of thermal degradation and estimation of lifetime for polypropylene particle: effect of particle size. Polym Degrad Stab. 2008;93:24–35.
32. Flynn JH. The 'Temperature Integral'—its use and abuse. Thermochim Acta. 1997;300:83–92.
33. Chrissafis K. Kinetics of thermal degradation of polymers. Complementary use of isoconversional and model-fitting methods. J Therm Anal Calorim. 2009;95:273–83.
34. Cadenato A, Morancho JM, Fernandez-Francos X, Salla JM, Ramis X. Comparative kinetic study of the non-isothermal thermal curing of bis-GMA/TEGDMA systems. J Therm Anal Calorim. 2007;89:233–44.
35. Su T-T, Jiang H, Gong H. Thermal stabilities and the thermal degradation kinetics of poly(ε-Caprolactone). Polymer-Plastics Technol Eng. 2008;47:398–403.
36. Senum GI, Yang RT. Rational approximations of the integral of the Arrhenius function. J Therm Anal. 1977;11:445–7.
37. Boonchom B, Puttawong S. Thermodynamics and kinetics of the dehydration reaction of $FePO_4{\cdot}2H_2O$. Phys B. 2010;405:2350–5.
38. Vlaev L, Nedelchev N, Gyurova K, Zagorcheva M. A comparative study of non-isothermal kinetics of decomposition of calcium oxalate monohydrate. J Anal Appl Pyrol. 2008;81:253–62.